

Computing magnetic anisotropy constants of single molecule magnets[†]

S RAMASESHA^{1,*}, SHAON SAHOO², RAJAMANI RAGHUNATHAN¹ and DIPTIMAN SEN³

¹Solid State and Structural Chemistry Unit, Indian Institute of Science, Bangalore 560 012

²Department of Physics, Indian Institute of Science, Bangalore 560 012

³Center for High Energy Physics, Indian Institute of Science, Bangalore 560 012

e-mail: ramasesh@sscu.iisc.ernet.in

Abstract. We present here a theoretical approach to compute the molecular magnetic anisotropy parameters, D_M and E_M for single molecule magnets in any given spin eigenstate of exchange spin Hamiltonian. We first describe a hybrid constant M_S -valence bond (VB) technique of solving spin Hamiltonians employing full spatial and spin symmetry adaptation and we illustrate this technique by solving the exchange Hamiltonian of the Cu_6Fe_8 system. Treating the anisotropy Hamiltonian as perturbation, we compute the D_M and E_M values for various eigenstates of the exchange Hamiltonian. Since, the dipolar contribution to the magnetic anisotropy is negligibly small, we calculate the molecular anisotropy from the single-ion anisotropies of the metal centers. We have studied the variation of D_M and E_M by rotating the single-ion anisotropies in the case of Mn_{12}Ac and Fe_8 SMMs in ground and few low-lying excited states of the exchange Hamiltonian. In both the systems, we find that the molecular anisotropy changes drastically when the single-ion anisotropies are rotated. While in Mn_{12}Ac SMM D_M values depend strongly on the spin of the eigenstate, it is almost independent of the spin of the eigenstate in Fe_8 SMM. We also find that the D_M value is almost insensitive to the orientation of the anisotropy of the core Mn(IV) ions. The dependence of D_M on the energy gap between the ground and the excited states in both the systems has also been studied by using different sets of exchange constants.

Keywords. Single molecule magnets; single-ion anisotropy; anisotropy parameters.

1. Introduction

There has been a widespread interest to develop molecule-based systems with magnetic ground state called single molecule magnets (SMMs). Following the synthesis of Mn_{12}Ac and Fe_8 clusters with high-spin ground state, exotic properties like Quantum Resonant Tunneling (QRT) and quantum coherence were unveiled.^{1–4} SMMs are characterized by a high spin ground state and large negative magnetic anisotropy (D_M) which creates an energy barrier between the states corresponding to positive and negative M_S values (figure 1).⁵ In this case, the magnetic anisotropy is said to be uniaxial and the ground state of the molecule would correspond to the highest possible magnetization with total spin S_{GS} . The second order transverse or rhombic anisotropy mixes various states with total spin S_{GS} that differ in their M_S value by two. Thus, in $S_{GS} = 10$ ground state, the

$M_S = +10$ and $M_S = -10$ states are connected through the E_M term in the tenth order. E_M will be non-zero only if the $S_X^2 - S_Y^2$ term remains invariant under the symmetry of the molecule. However, fourth order anisotropy terms need to be included in the anisotropy Hamiltonian for Mn_{12}Ac in which the molecular symmetry prohibits a non-zero E_M but still QRT

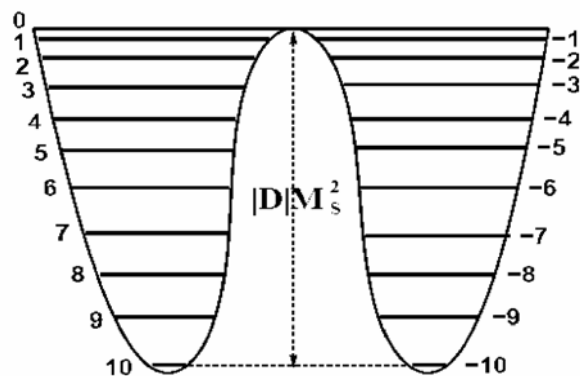


Figure 1. Schematic of the double potential well for the $S_{GS} = 10$ ground state when D_M is negative.

[†]Dedicated to the memory of the late Professor S K Rangarajan

*For correspondence

is observed. The requirement of large negative value of D_M and a large non-zero ground state spin are stringent requirements for a molecule to behave as a SMM. Modelling magnetic anisotropy in these systems becomes necessary for developing new SMMs with desired properties.

Magnetic anisotropy of SMMs is computed by treating the anisotropy Hamiltonian as a perturbation over the Heisenberg exchange Hamiltonian, since the magnitude of anisotropy constants are very small compared to the exchange constants. SMMs contain many spin centers with equal or unequal magnitude of site spins and in most cases the magnetic exchange is frustrated. The Fock space of the Hamiltonian for even the well known SMMs are generally very large (hundred million in case of $\text{Mn}_{12}\text{Ac}^6$ and more than two billion in the case of Fe_{12} wheel⁷) and obtaining even a few low-lying states of the Hamiltonian could pose a serious computational challenge. Since the exchange Hamiltonian conserves both total spin and z -component of total spin (M_S), the problem can be simplified by specializing the basis.

Hamiltonian could be block diagonalized in spin-adapted or constant M_S basis, so that one can work with a basis set with a particular total spin or M_S value. This can be further simplified by exploiting spatial symmetries of the model. An ideal situation would correspond to one in which all the spin and spatial symmetries are utilized to construct a fully symmetrized basis to minimize the size of the Hamiltonian matrix that needs to be diagonalized. Besides the computational efficiency, this method of solving the model Hamiltonian enables us to label the states by the irreducible representation which they belong to. In the succeeding sections of this paper, we present the technique of solving spin Hamiltonians using spin and spacial symmetry adaptation. Then we discuss a theoretical approach to compute molecular magnetic anisotropy in SMMs.

2. Solving exchange Hamiltonian

The constant M_S basis can be trivially constructed from the Fock space by choosing those states whose total M_S value corresponds to the desired value. It is also quite straightforward to set up the Hamiltonian matrix in this basis and solve for a few low-lying states in cases where the Hilbert space is spanned by a few hundred million states.⁸ It is computationally difficult to solve systems with magnetic frustration. In such systems, the ground state spin is often not

predictable and one needs to obtain the lowest state in each total spin subspace to fix the spin of the ground state. Besides, it is also numerically difficult to achieve convergence to nearly degenerate eigenstates with different spin values, unless they can be dispersed into orthogonal Hilbert spaces. We can partially alleviate this problem by employing the parity symmetry of the exchange Hamiltonian. This symmetry can break the $M_S = 0$ space into even and odd total spin subspaces.⁹ Since in most cases, the lowest excited state usually has a spin which is one different from that of the ground state, this symmetry makes it easy to obtain the spin gaps accurately.

Construction of spin adapted configuration state functions (CSFs) has been a long standing problem of interest. The CSFs are simultaneous eigenstates of total S_{tot}^2 and S_{tot}^z and setting up the Hamiltonian matrix in this basis leads to matrices of smaller size besides allowing automatic labelling of the states by the total spin. Furthermore, the eigenvalue spectrum is enriched, since we can obtain several low-lying states in each total spin sector. This is in contrast to obtaining several low-lying states in a given total M_S sector as the latter would have states with total spin $S_{\text{tot}} \geq M_S$. There are many ways of achieving CSFs.¹⁰ The methods which have been in extensive study are (i) the graphical unitary group approach (GUGA), (ii) symmetry group graphical approach (SGGA) and (iii) valence-bond (VB) approach. Complete factorization of the Hilbert space of the Hamiltonian using both spin and spatial symmetries has been the focus of many studies.⁹ However, exploitation of spatial and spin symmetries has been possible only for Abelian point groups. Here we present a general technique which is a hybrid method based on Valence-bond basis and the basis of z -component of the total spin, which is applicable to all types of point groups and is easy to implement on computer. But, before that we will briefly discuss a previous attempt to symmetrize VB basis¹¹ and associated difficulties.

2.1 Symmetrized VB approach

Its is non-trivial to get simultaneous eigenstates of total spin and its z -component, since eigenstates of the S_{tot}^z operator expressed as a product of the eigenstates of all the S_i^z operators are not simultaneously eigenstates of the S_{tot}^2 operator. The situation is further complicated by the fact that in a molecular magnet, often the spins of all the constituent mag-

netic centers, s_i are not the same. In such a case, the easiest way of constructing the spin adapted functions is the diagrammatic valence bond (VB) method based on modified Rumer–Pauling rules.^{12–15} In this method, a magnetic site with a given spin ‘ s_i ’ is replaced by $2s_i$ spin-half objects. To obtain a state with total spin S from N such spin-1/2 objects from all the magnetic centers, $(N - 2S)$ of these spin-1/2 objects are singlet spin paired explicitly, subject to the following restrictions: (1) there should be no singlet pairing of any two spin-half objects belonging to the same magnetic center (this ensures that the $2s_i$ objects are in a totally symmetric combination¹⁶), (2) a total of $2S$ spin-half objects are left unpaired, (3) when all the spin-half objects are arranged at the vertices of a regular polygon with number of vertices equal to number of spin-half objects, N , and straight lines are drawn between spin paired vertices, there should be no intersecting lines in the resulting diagram and (4) when all the spin-half objects are arranged on a straight line and lines are drawn between spin paired objects, these lines should not enclose any unpaired spin-1/2 object. These rules follow from the generalization of the Rumer–Pauling rules to objects with spin greater than 1/2 and total spin greater than zero. The set of diagrams which obey these rules would hence forth be called ‘legal’ VB diagrams. Some legal VB diagrams are shown in figure 2.

A line in the VB diagram between two spin $-1/2$ objects i and j corresponds to the state $(\alpha_i\beta_j - \beta_i\alpha_j)/\sqrt{2}$ where we choose α to correspond to $|\uparrow\rangle$ and β to $|\downarrow\rangle$ orientations of the spin. The phase convention assumed is that the ordinal number ‘ i ’ is less than the ordinal number ‘ j ’. The $2S$ spin-1/2 objects $k_1 k_2$

$k_3 \dots k_{2S}$ which are left unpaired can be taken to represent the state with $M_S = S$ given by $\alpha_{k_1}\alpha_{k_2}\alpha_{k_3}\dots\alpha_{k_{2S}}$. VB states corresponding to other M_S value for this state with spin S , can be obtained by operating the S_{tot} operator on the state by the required number of times. The VB state corresponding to a given diagram is a product of the states representing the constituent parts of the diagram. On a computer, a ‘legal’ VB diagram of any spin can be uniquely represented by an integer of N bits with a bit state ‘1’ at a site representing the beginning of a singlet line and a state ‘0’ the ending of a singlet line. The unpaired spins are also represented as one-bits. Figure 2 also shows bit representation of typical VB diagrams.

To spatially symmetrize a VB basis, it is necessary to know the result of a symmetry operator operating on a legal VB diagram. Unfortunately this leads to ‘illegal’ VB diagrams, decomposing them into ‘legal’ ones is computationally demanding. An example of this is shown in figure 3.¹¹ In practice, the VB space is broken down into smaller invariant subspaces by the actions of group operations and then disjoint invariant subspaces are identified. Within each disjoint invariant space, a symmetrized linear combination of the VB basis is constructed by the application of projection operator. However, the structure of the invariant spaces is very complex and constructing disjoint invariant spaces is not simple.¹¹ While the number of linearly independent symmetry combinations of a given representation is known a priori, the actual linear combinations are obtained by carrying out Gram–Schmidt orthonormalization of the projected states. However, since the VB diagrams are not orthogonal the orthonormalization process is both computationally involved and time consuming. Furthermore, in case of molecular magnets containing magnetic ions with spin greater than half, the exchange operator between such high spin centers also generates ‘illegal’ VB diagrams as it involves non-nearest neighbour exchange interactions between constituent elementary spins.^{9,14,15}

In view of these difficulties, a fully symmetrized VB approach to solving Heisenberg exchange Hamiltonian particularly in the context of molecular magnets is not feasible.

2.2 Hybrid method based on VB basis and constant M_S basis

In the constant M_S basis, a basis state of an ensemble of spins s_1, s_2, \dots, s_N , is represented by a direct

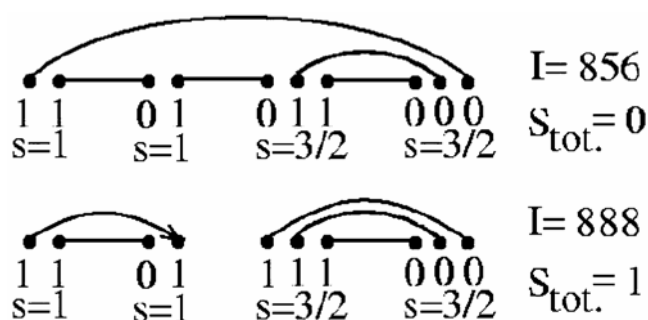


Figure 2. The top VB diagram shows spin pairings to yield a total spin $S_{\text{tot}} = 0$ state from ten spin-1/2 objects, constituent elementary spins of two spin 1 and two spin 3/2. Its bit representation corresponds to unique integer $I = 856$. The bottom VB diagram shows a $S_{\text{tot}} = 1$ state, the corresponding unique integer is $I = 888$.

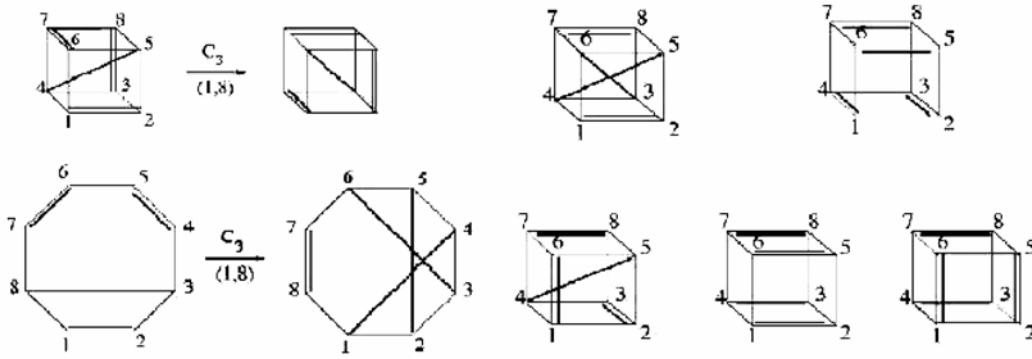


Figure 3. The effect of operation by the C_3^1 symmetry operator about the (1, 8) axis. Top left shows the initial and final VB diagrams with spin couplings between vertices of the cube shown as dark lines. Bottom left shows the same states as spin couplings between vertices of a regular octagon. The resultant is an ‘illegal’ diagram. Decomposing the resultant to ‘legal’ VB diagrams yields a sum of five VB diagrams shown on the right, with spin couplings between vertices on a cube.

product of the m_s states of each spin such that the total $M_S = \sum m_i$. By construction the states are orthonormal. A VB diagram with p singlet lines can be broken up into a linear combination of 2^p basis states in the constant M_S basis. In conversion of VB diagrams to constant M_S basis, each singlet line gives two states; in one, the site at which a singlet line begins is replaced by an α spin and the site at which the line ends is replaced by a β spin with phase factor $+1$ and in the other state, spins are reversed with an associated phase of -1 . However, there is a normalization constant w_i , which follows from Clebsch–Gordan coefficients, given by,

$$w_i = \left[\frac{(2s_i)!}{(s_i + m_i)!(s_i - m_i)!} \right]^{-1/2}, \tag{1}$$

for a site with composite spin s_i in state m_i , given by, $m_i = (n_{i\uparrow} - n_{i\downarrow})/2$. Here, $n_{i\uparrow}$ is the number of $m = +1/2$ and $n_{i\downarrow}$ is the number of $m = -1/2$ constituent spins at the i th site.¹⁶ Without loss of generality, we can assume that the M_S value of the VB diagram is also S . It is computationally straightforward to express a state in the VB basis as a linear combination of states in the constant M_S basis. We initialize the coefficients in the constant M_S basis to zero. We then decompose, sequentially, each VB diagram into constant M_S states and update the coefficient of the basis state of corresponding M_S by adding to it the VB coefficient times the product of Clebsch–Gordan factors with appropriate phases. The matrix relating the VB basis states to constant M_S basis states, C , is a $V \times M$ matrix, where V is the dimensionality of the VB space and M that of the constant M_S space.

In the constant M_S basis, we can get the matrix representation of a symmetry operator, \hat{R} of the point group in the chosen M_S space by operating with \hat{R} on each state and searching for the resulting state in the list of M_S basis states. Each basis state in this representation is carried over to another basis state by a symmetry operation of the point group. Thus, the matrix R_M though an $M \times M$ matrix contains only one non-zero element in each row; this makes manipulations with this matrix computationally fast. The knowledge of the C and the R_M matrices give the effect of operating by the symmetry operator \hat{R} on a VB state as a linear combination of the constant M_S basis states via the matrix $B_R = CR_M$.

The projection operator for projecting out the basis states on to a chosen irreducible representation of the point group Γ is given by,

$$P_\Gamma = \sum_R \chi_\Gamma^{\text{irr}}(\hat{R})\hat{R}, \tag{2}$$

where $\chi_\Gamma^{\text{irr}}(\hat{R})$ is the character under the symmetry operation \hat{R} in the character table of the point group of the system.¹⁷ In our approach, one can easily get the effect of projection operator on VB states, expressed in constant M_S basis. The matrix representation of P_Γ , obtained in the mixed VB and constant M_S basis is given by,

$$Q_\Gamma = \sum_R \chi_\Gamma^{\text{irr}}(R)B_R, \tag{3}$$

where, Q_Γ is a $V \times M$ matrix. However, the rows of the matrix Q_Γ are not all linearly independent. The

exact dimension, V_Γ , of the Hilbert space spanned by the system in the irreducible representation Γ can be known *a priori*, which is given by,

$$V_\Gamma = (d_\Gamma/h) \sum_{\hat{R}} \chi(\hat{R}) \chi_\Gamma^{\text{irr}}(\hat{R}), \quad (4)$$

where d_Γ is the dimensionality of the irreducible representation Γ , h is the number of elements in the point group and $\chi(\hat{R})$ is the reducible character for the operation \hat{R} . The $V_\Gamma \times M$ projection matrix, P_Γ of rank V_Γ is obtained by Gram–Schmidt orthonormalization of the rows of the matrix Q_Γ until V_Γ orthonormal rows are obtained. The $M \times M$ Hamiltonian matrix, H_M is constructed in the constant M_S basis which is described elsewhere.⁸ The projected $V_\Gamma \times V_\Gamma$ Hamiltonian matrix in the fully symmetrized basis is given by,

$$H_\Gamma = P_\Gamma H_M (P_\Gamma)^\dagger, \quad (5)$$

and one could use any of the well-known full diagonalization routines to obtain the full eigenspectrum or use the Davidson algorithm to get a few low-lying states of the symmetrized block Hamiltonian in the chosen spin and symmetry subspace.

We can further reduce dimensions of the blocks of Hamiltonian corresponding to E , T or higher order representations, which give degenerate eigenvalues. In such cases, it is advantageous to work with bases that transform according to one of the components of the irreducible representation. This will lead to unique eigenvalues. To achieve this, we choose an axis of quantization and project out basis states of the irreducible representation which are diagonal about a rotation about the chosen axes. For example, in the case of the irreducible representation that transforms as T , we can choose one of the C_3 axes as a quantization axis and project the basis states of the irreducible representation using $(I + C_3^1 + C_3^{-1})$ as the projection operator. This operator projects states that transform as the Y_1^0 component of the three fold degenerate irreducible tensor operator. Similarly, for the E representation, we could use any of the C_2 axis as a quantization axis and use the projection operator $(I + C_2^1)$ to project out basis states that transform as one of its components.

2.2a Discussion on hybrid method: Computationally, this hybrid method involves few more steps than that of only constant M_S method.⁹ Firstly, we

need to construct the C matrix, whose i th row contains the coefficients of the constant M_S functions appearing in the i th VB basis function. This is a pretty fast step as the constant M_S states are an ordered sequence of integers and a VB state with n lines is a linear combination of $2n$ constant M_S functions. Secondly, in the hybrid approach, the computation of the Q matrix involves the matrix multiplication,

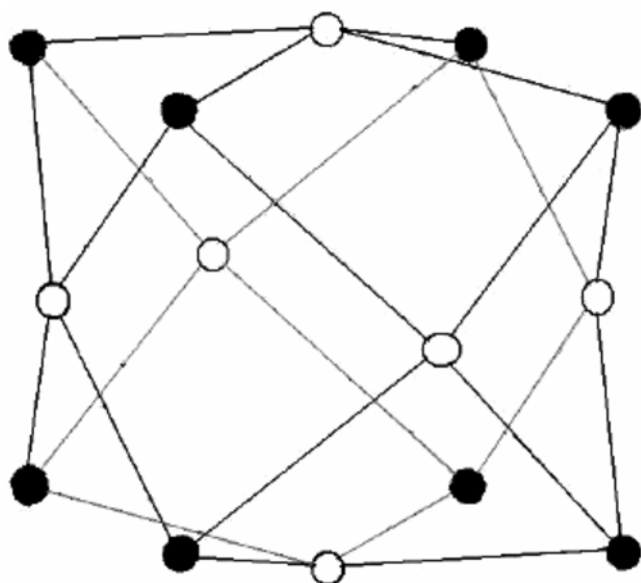
$$C \left(\sum_R \chi_\Gamma^{\text{irr}}(R) R_M \right) = C R'_M.$$

The number of arithmetic operations involved is however very small, since both C and R'_M are sparse matrices. Gram–Schmidt orthonormalization for obtaining the projection matrix P_Γ from the Q matrix in the hybrid approach and from R'_M matrix in constant M_S approach – both involve similar computational effort. The advantage of fewer orthonormal rows being sought for P_Γ in the hybrid approach compared to the projection matrix in the constant M_S approach is compensated by the loss of sparseness of Q matrix in the hybrid approach. Computation of the eigenvalues in the constant MS approach is slower than in the hybrid approach, since $(D(\Gamma_{M_S}) > D(\Gamma_S))$ for most S , where $D(\Gamma_S)$ is the dimensionality of the space of the irreducible representation Γ with spin S and $D(\Gamma_{M_S})$ is similarly the dimension of the space Γ with constant M_S . The memory required for the hybrid approach is not very different from that of constant M_S approach since the matrices though smaller in the hybrid approach, are slightly denser. The only additional array required to be stored in the hybrid approach is the sparse C matrix.

The major advantage of the hybrid approach is that we can obtain a far richer spectrum, since we are targeting each spin sector separately, unlike in the constant M_S approach. Thus, if we can obtain, say 10 states in each S sector of the $2n$ spin-1/2 problem, we would have $10(n+1)$ unique states compared to the constant M_S technique where many of these spin states would be repeated in different M_S sectors. This approach is applicable not only to spin systems, it can be easily extended to electronic systems as well. Indeed, in table 1, we show the break-up of the many body states of a π -system, made up of sp^2 carbon atoms placed at the vertices of an icosahedron, into various subspaces of I_{mnh} for different total spin values.

Table 1. Dimensionalities of various subspaces of half-filled icosahedral electronic system.

$S_{\text{tot}} \rightarrow$							
$\Gamma \downarrow$	0	1	2	3	4	5	6
A_g	2040	3128	1684	382	38	3	1
T_{1g}	16602	28821	14625	3261	309	6	0
T_{2g}	16602	28821	14625	3261	309	6	0
G_g	30272	50932	26236	5880	568	16	0
H_g	47940	79305	41255	9220	900	40	0
A_u	1852	3188	1644	348	40	0	0
T_{1u}	17080	28686	14700	3372	294	18	0
T_{2u}	17080	28686	14700	3372	294	18	0
G_{2u}	30160	50992	26176	5888	560	16	0
H_u	46880	79680	40980				
Tot Dim \rightarrow	226512	382239	196625	44044	4212	143	1

**Figure 4.** Schematic of Cu_6Fe_8 cluster. Filled and open circles correspond to Fe and Cu (both spin-1/2) sites respectively. Lines represent the exchange coupling between various spin sites.

In this approach, we have demonstrated, how by combining the ease of spin symmetry adaptation of the VB method with the spatial symmetry exploitation of the constant M_S methods, we can devise a scheme which is fully spin and spatial symmetry adapted. This has been possible because of the ease of transformation of the VB basis to the constant M_S basis. The method described here can easily be extended to fermionic systems and should provide a significant improvement for obtaining exact eigenstates of spin conserving model Hamiltonians. In the next section, we have demonstrated the power of the

method by applying it to the exchange Hamiltonian of the molecular magnet Cu_6Fe_8 which has cubic symmetry.

2.2b Application to Cu_6Fe_8 : We have applied the above method to model the susceptibility behaviour of the molecule $[(\text{Tp})_8(\text{H}_2\text{O})_6\text{Cu}_6^{\text{II}}\text{Fe}_8^{\text{III}}(\text{CN})_{24}(\text{ClO}_4)_4 \cdot 12\text{H}_2\text{O} \cdot 2\text{Et}_2\text{O}]^{18}$ where Tp stands for hydrotris (pyrazolyl) borate (figure 4). In this molecule, both Cu^{II} and Fe^{III} ions are in spin-1/2 state. The eight Fe^{III} ions are at cube corners and the six Cu^{II} ions are on the outward perpendicular to the face centers of the cube. Each Cu^{II} ion is connected to the four nearest Fe^{III} ions via ferromagnetic exchange interactions. There are no Fe–Fe or Cu–Cu interactions. This system has a very high symmetry of the cube and incorporates all the complexities that can be encountered in the application of our technique. From the susceptibility data, the strength of the exchange interaction J , was estimated to be 30 cm^{-1} .¹⁸ The dimensions of the various subspaces are given in table 2. Using the hybrid method, we have broken down the space in each total spin sector into basis states that transform as different irreducible representations of the cubic point group.

The dimensionalities of the various subspaces are shown in table 3. The subspaces transforming as the E or T representations are further broken down as we discussed before. We have setup the Hamiltonian matrix in each of the subspaces and obtained all the eigenvalues. We have also used a constant M_S basis and using the full cubic symmetry, factored the space into various irreducible representations and obtained all the eigenvalues in each subspace. From the eigenvectors, we have computed the total spin of

Table 2. Dimensionalities of the total spin spaces of a system of 14 spin-1/2 objects. $D(S)$ is the dimensionality of the constant S basis and $D(M_S)$ is the dimensionality of the constant M_S basis.

S/M_S	0	1	2	3	4	5	6	7
$D(S)$	429	1001	1001	637	273	77	13	1
$D(M_S)$	3432	3003	2002	1001	364	91	14	1

Table 3. Dimensionalities of various subspaces of the $\text{Cu}_6^{\text{II}}\text{Fe}_8^{\text{III}}$ cluster for irreducible representation.

$S_{\text{tot}} \rightarrow$ $\Gamma \downarrow$	0	1	2	3	4	5	6	7
A_{1g}	6	32	24	24	9	5	1	1
A_{2g}	13	15	19	8	5	0	0	0
E_g	34	90	90	60	26	10	2	0
T_{1g}	78	165	171	99	39	6	0	0
T_{2g}	66	216	186	138	54	21	3	0
A_{1u}	5	19	13	11	2	0	0	0
A_{2u}	17	20	27	15	10	2	1	0
E_u	36	78	84	48	20	6	0	0
T_{1u}	105	180	219	123	66	15	6	0
T_{2u}	69	186	168	111	42	12	0	0

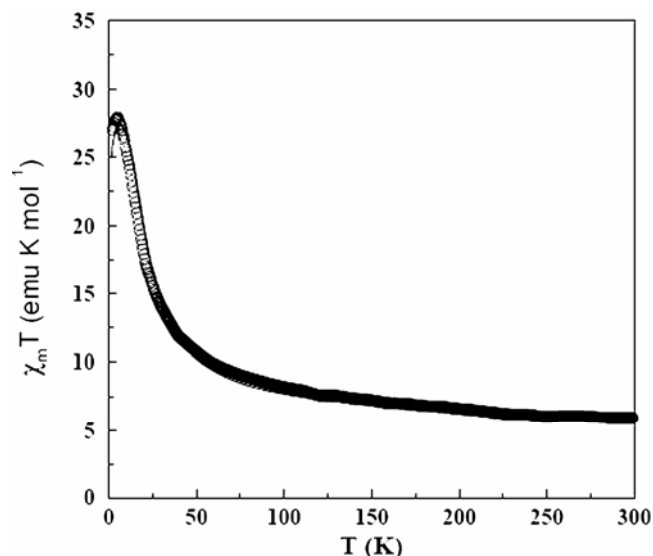
the state. We find a one to one correspondence to numerical accuracy, between the two sets of calculations. We have also fitted the χT vs T experimental plot by using the full spectrum of the Heisenberg Hamiltonian and computing¹⁹

$$\chi T = \frac{3}{8} \left[\frac{g^2 F(J, T)}{1 - zJF(J, T)/k_B T} \right], \quad (6)$$

where we have taken the g factor to be 2.1, the ferromagnetic exchange constant J to be 27.2 cm^{-1} . Here, χT is in units of $N\mu_B$. The function $F(J, T)$ is given by,

$$F(J, T) = \frac{\sum_{S, M_S} M_S^2 \exp[-E_0(S, M_S)/k_B T]}{\sum_{S, M_S} \exp[-E_0(S, M_S)/k_B T]}, \quad (7)$$

with $E_0(S, M_S)$ being the eigenvalue of the sum of exchange Hamiltonian and the magnetic anisotropy term DS_Z^2 and zJ is the intermolecular exchange interaction. Here we have assumed that the molecular anisotropy is along the global z -axis, and this term is treated as a perturbation to the exchange Hamiltonian in (1). In figure 5, we show the fit of the experimental data to the model.

**Figure 5.** Fit of the χT vs T plot for the $\text{Cu}_6^{\text{II}}\text{Fe}_8^{\text{III}}$ cluster. The best fit parameters are, $J = 27.2 \text{ cm}^{-1}$ (ferromagnetic), $zJ' = -0.008 \text{ cm}^{-1}$ (antiferromagnetic), $D = -0.15 \text{ cm}^{-1}$ and $g = 2.1$.

3. Computing magnetic anisotropy in SMMS

The magnetic anisotropy is given by the general Hamiltonian,

$$\hat{H}_D = \hat{S}_M \cdot D^{(M)} \cdot \hat{S}_M, \quad (8)$$

where \hat{S}_M corresponds to the spin operator for the total spin of the molecule and $D^{(M)}$ is the magnetic anisotropy tensor of the molecule. In practice, this $D^{(M)}$ tensor is diagonalized and the eigenvalues of the tensor give magnetic anisotropy in three mutually perpendicular principal directions while the eigenvectors corresponds to the direction of orientation of the principal axes with respect to the molecular frame. If, D_{XX}^M , D_{YY}^M and D_{ZZ}^M are the molecular anisotropies along the three principal directions such that $D_{XX}^M + D_{YY}^M + D_{ZZ}^M = 0$, we can define two parameters, D_M and E_M such that,

$$D_M = D_{ZZ}^M - \frac{1}{2}(D_{XX}^M + D_{YY}^M)$$

$$E_M = \frac{1}{2}(D_{XX}^M - D_{YY}^M), \quad (9)$$

where D_M and E_M are called the axial and rhombic anisotropies respectively. Using these two parameters, the Hamiltonian in (8) can be rewritten as,

$$H_M = D_M(\hat{S}_Z^2 - S(S+1)) + E_M(\hat{S}_X^2 - \hat{S}_Y^2). \quad (10)$$

The magnetic anisotropy could be of relativistic or dipolar origin. In systems like conjugated polymers, the anisotropy arises due to the dipolar interactions, whereas in SMMs containing transition metal ions, relativistic effects dominate and the dipolar contribution to anisotropy is two to three orders of magnitude smaller. There have been several theoretical methods to compute the molecular magnetic anisotropy in molecular magnets. The first method involves computing the D_M and E_M values by tensorial summation of the anisotropies of the constituent transition metal centers.^{20–22} However, this leads to molecular anisotropy values which are independent of the total spin state of the molecule. The next method involves computation of $D^{(M)}$ tensor using the effective mean-field potential $\varphi(r)$ obtained from density functional theory (DFT) with desired S_Z^{total} of the cluster. Treating spin orbit (SO) operator, $\hat{S} \cdot [\hat{p} \times \hat{\nabla} \Phi(\vec{r})]$ as a perturbation, the $D^{(M)}$ tensor is obtained.^{23–27} However, DFT methods do not conserve either the total spin or the site spins. Thus, it is not possible to obtain a pure spin eigenstate. Moreover, mean-field theories do not give correct values of spin–spin correlations. There have been methods to obtain the single-ion anisotropy values using restricted configuration interaction approach.²⁸ Bencini

and Gatteschi developed a perturbative technique to obtain the anisotropy values of bi-nuclear systems. This method is analytical and cannot be employed for larger systems like Mn_{12}Ac and Fe_8 clusters.

Here, we present a general method to compute magnetic anisotropy of large cluster of ions with arbitrary spins in any given total spin state. We use a spin-exchange Hamiltonian to describe the cluster, unlike the all electron Hamiltonian that is employed in DFT studies. We obtain desired exact eigenstates of the exchange Hamiltonian by methods described above and using the magnetic anisotropic interactions as a perturbation to compute the molecular anisotropy constants in the desired eigenstates, in first order in perturbation. The input parameters required in our study are the local single ion anisotropies and the exchange constants of the exchange Hamiltonian. Our study can yield the anisotropy values for different total spin states as well as for different states with the same total spin. In the next section we describe the method in detail. In the following section we present the results of our studies on the two SMMs, Mn_{12}Ac and Fe_8 and finally we summarize our studies.

3.1 Methodology

We treat the exchange Hamiltonian between magnetic centers in the SMMs as the unperturbed Hamiltonian,

$$\hat{H}_0 = \sum_{\langle ij \rangle} J_{ij} \hat{S}_i \cdot \hat{S}_j, \quad (11)$$

where $\langle ij \rangle$ runs over all pairs of centers in the model for which the exchange constant is non-zero, \hat{S}_i is the spin on the i th magnetic center. In SMMs such as Mn_{12}Ac the spins at all the magnetic centers are not the same and the exchange interactions are shown in figure 6. H_0 can be solved exactly for a few low-lying states in a chosen spin sector by using methods that have been described above.⁹

The general anisotropic Hamiltonian for a collection of magnetic centers \hat{H}'_1 is given by,

$$\hat{H}'_1 = \frac{1}{2} \sum_{i,j,\alpha,\beta} D_{ij,\alpha\beta} \hat{S}_i^\alpha \hat{S}_j^\beta, \quad (12)$$

where the indices i and j run over all the magnetic centers and α and β run over x , y and z directions of the ion. The contributions to inter-center anisotropy

constant arise due to dipolar interaction between the spins on the two centers as well as due to relativistic effects. In the former, $D_{ij,\alpha\beta}$ is given by,

$$D_{ij,\alpha\beta} = \frac{1}{2} g^2 \mu_B^2 \left\langle \frac{\Re_{ij}^2 \delta_{\alpha\beta} - 3R_{ij,\alpha} R_{ij,\beta}}{R_{ij}^5} \right\rangle, \quad (13)$$

where $\Re_{ij}(R_{ij})$ is the vector (distance) between the magnetic centers i and j , g is the gyromagnetic ratio and μ_B is the electronic Bohr magneton; the expectation value in (13) is obtained by integration over spatial coordinates.²⁹ Approximating the expectation values of the distances by the equilibrium distances, the $D_{ij,\alpha\beta}$ in (13) and by computing the necessary spin–spin correlation functions, we can obtain the molecular $D_{\alpha\beta}^{(M)}$ tensor.³⁰ The eigenvalues of this matrix give the principal anisotropy values and imposing the condition of zero trace of the matrix yields molecular magnetic anisotropy constants due to spin–spin interactions. The magnetic anisotropies computed assuming only spin dipolar interactions yielded negligibly small values in comparison to the experimentally observed $D_M = -0.7$ K and -0.28 K for Mn_{12}Ac and Fe_8 SMMs respectively, in the $S = 10$ ground state.^{31,32} Thus, we need to compute the magnetic anisotropy of SMMs from the single-ion anisotropies of the constituent magnetic centers since, in SMMs relativistic effects dominate due to the presence of transition metal ions. The relativistic

interactions are short-ranged, they fall off as r^{-3} . Hence in (12), we can ignore inter-site terms and replace \hat{H}'_1 by \hat{H}_1 given by,

$$\hat{H}_1 = \sum_{i,\alpha,\beta} D_{i,\alpha} \hat{S}_i^\alpha \hat{S}_i^\beta. \quad (14)$$

Since, the local anisotropies of the individual ions can have their own set of principal axes, we need to project out the components of anisotropy on to the laboratory axes. This modifies the (14) to

$$\hat{H}_1 = \sum_{i,\alpha,\beta,l,m} C_{i,l\alpha} C_{i,m\beta} D_{i,\alpha\beta} \hat{S}_i^\alpha \hat{S}_i^\beta, \quad (15)$$

where, $C_{i,l\alpha}$ is the direction cosines of α th coordinate of the local axis of the i th magnetic center with the l th coordinate of the laboratory frame. Since, the Hamiltonians in (8) and (15) are equivalent, we can equate the matrix elements $\langle n, S_M, S | \hat{H}_1 | n, S_M, S' \rangle$ and $\langle S_M, S | \hat{H}_D | S_M, S' \rangle$ and for any pair of eigenstates of the exchange Hamiltonian in (11); M and M' are z-component of total spin in a state n with spin S_M in which we are interested. Calculating these matrix elements for \hat{H}_D is straightforward from the algebra of spin operators. However, evaluation of the matrix elements of \hat{H}_1 between eigenstates of \hat{H}_0 , requires a knowledge of the matrix elements of different products of site spin operators (such as $\hat{S}_i^x \hat{S}_j^y$). For this we need eigenstate of \hat{H}_0 , $|n, S, M\rangle$, for different M values and these are obtained by using the ladder operators corresponding to spin S .

Given a S value, the above condition would give rise to $(2S + 1)^2$ equations, while the tensor $D^{(M)}$, has only nine unknowns corresponding to the nine components of the second rank tensor. Thus, for the Mn_{12}Ac system, with ground state spin of 10, there would be 441 equations and we have more equations than unknowns. However, we could take any nine equations and solve for the components of the tensor $D^{(M)}$ and we would get unique values of the components. This is guaranteed by the Wigner–Eckart theorem and we have also verified this by solving for the $D^{(M)}$ tensor from several arbitrarily different selections of the nine equations.

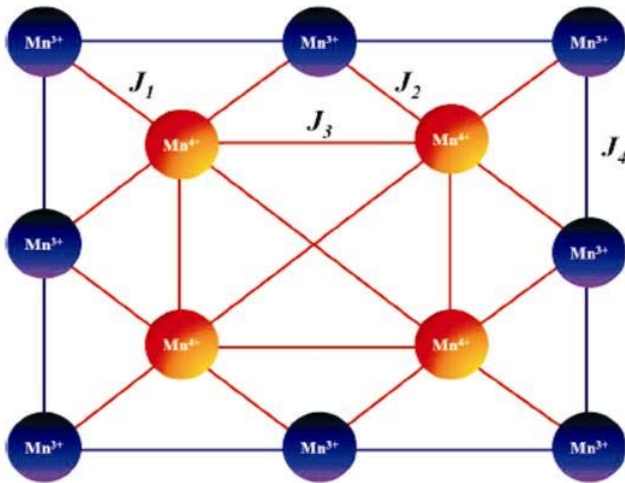


Figure 6. Schematic of possible exchange interactions in Mn_{12}Ac SMM. The peripheral Mn(III) ions represented by blue circles correspond to spin-2 sites and those represented by yellow circles are the core Mn(IV) ions each of spin-3/2. J_s are the strength of superexchange interaction with $J_1 = 215$ K, $J_2 = J_3 = 85.6$ K, $J_4 = -64.5$ K.⁶

3.2 Results and discussion

We have computed D_M and E_M values for both Mn_{12}Ac and Fe_8 systems by systematically rotating the local anisotropies of the spin centers. We have

used the single-ion anisotropy values quoted in the literature for the magnetic ions in similar ligand environments.^{33–36} The local ion axis referred to as x , y and z and the laboratory axis denoted by X , Y and Z are shown in figure 7. The laboratory frame can be arbitrarily chosen since, while computing the molecular anisotropy, we diagonalize the anisotropy tensor and obtain the anisotropy values along the three principal directions. The principal axis of the molecule is unique and it does not depend on the orientation of the laboratory axis.

In order to obtain the molecular anisotropy as a function of the angle θ which the z -axis of the ion makes with the laboratory Z -axis, we rotate the single-ion orientation with respect to the laboratory frame. The orientation of z -component of the single-ion anisotropy at every site is shown in figures 8, 9 and 10 (schemes 1, 2 and 3) for Mn_{12}Ac and in figures 14, 15 and 16 (schemes 4, 5 and 6) for Fe_8 systems respectively. First the z -axis (\bar{z}) of the ion is fixed and then \bar{x} is obtained by Gram-Schmidt orthogonalization procedure. Though the choice of this vector is arbitrary in a plane perpendicular to z -axis, we have fixed the direction of \bar{x} such as to have maximum projection along a $\text{M}-\text{O}$ ($\text{M} = \text{Mn}, \text{Fe}$) bond in Mn_{12}Ac as well as in Fe_8 (figures 7 and 16). If \vec{O} is the vector connecting a M site and a neighbouring O ion, then we obtain \bar{x} using the relation,

$$\bar{x} = \vec{O} - (\vec{O} \cdot \bar{z})\bar{z}. \quad (16)$$

Finally, the y -axis of the ion is obtained using the relation, $\bar{y} = \bar{z} \times \bar{x}$. These three mutually orthogonal vectors are then normalized to obtain the orthonormal set of coordinate axes x , y and z of the ion center. These single-ion axes of a given site i can be projected on to the laboratory frame through the direction cosines, $C_{i,\alpha\beta}$, where, $\alpha = X, Y, Z$ and $\beta = x, y, z$ (17).

$$\begin{aligned} x &= C_{i,Xx}X + C_{i,Yx}Y + C_{i,Zx}Z \\ y &= C_{i,Xy}X + C_{i,Yy}Y + C_{i,Zy}Z \\ z &= C_{i,Xz}X + C_{i,Yz}Y + C_{i,Zz}Z. \end{aligned} \quad (17)$$

3.2a *Magnetic anisotropy in Mn_{12}Ac SMM:* We have first obtained the ground state and few excited states of the Mn_{12}Ac system by exactly solving the

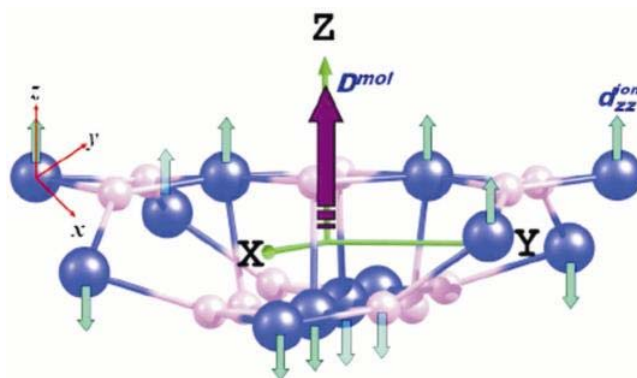


Figure 8. Schematic diagram showing the directions of local anisotropy in Mn_{12}Ac . The single-ion anisotropies of all the Mn ions are directed along the laboratory Z axis (scheme 1).

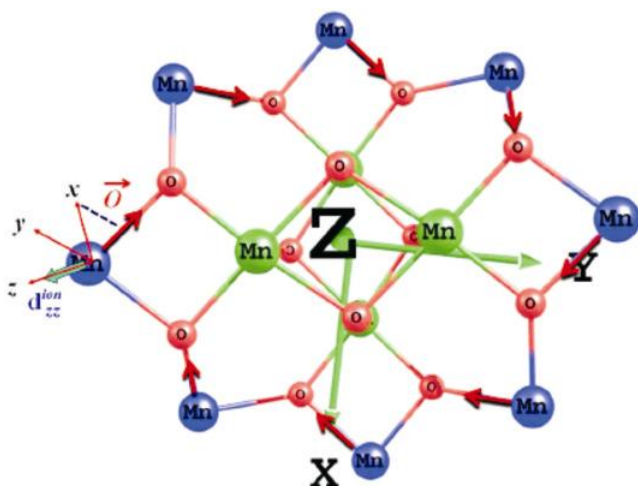


Figure 7. Schematic of local (x , y , z) and laboratory (X , Y , Z) coordinate axes in Mn_{12}Ac . The blue, green and red spheres correspond to Mn(III) (spin-2), Mn(IV) (spin-3/2) and oxygen ions respectively. The arrows indicate the Mn–O bonds on which the chosen local x -axis has maximum projection.

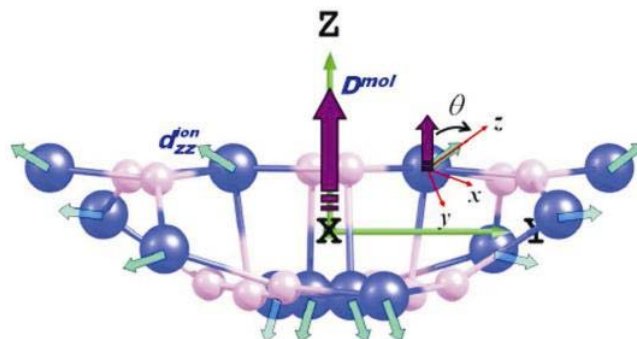


Figure 9. Schematic diagram showing the directions of local anisotropy in Mn_{12}Ac . The z -component of the single-ion anisotropies of all the Mn(III) ions are inclined at an angle θ to the laboratory Z and while that of the Mn(IV) ions are kept fixed at $\sim 48^\circ$ (scheme 2).

unperturbed Hamiltonian given in (11), using the exchange interactions shown in figure 6.⁶ The ground state of the system corresponds to total spin 10 with a total spin 9 first excited state at 35.1 K from the ground state and a $S = 8$ second excited state at 60.4 K from the ground state. The molecular magnetic anisotropy is computed using the single-ion anisotropy values of -5.35 K and 1.226 K respectively for Mn(III) and Mn(IV) ions, obtained from the literature. We have also introduced transverse anisotropy of 0.022 K and 0.043 K for Mn(III) and Mn(IV) ions respectively. We have studied the variation of molecular anisotropy as a function of orientation of the local anisotropies by rotating the local D tensor around the molecular Z -axis (refer figures 8–10). In scheme 1, all the single-ion z axes are pointed parallel to the laboratory Z direction while in scheme 2 the orientation of the local anisotropies of the core Mn(IV) ions are along the line joining the ion and the molecular center ($\sim 48^\circ$ from the laboratory Z -axis), while that of the Mn(III) ions is kept fixed at an angle θ from the Z axis. The orientation of the local anisotropy of Mn(III) ions for which we get the best agreement with experiments corresponds to $\theta \sim 17^\circ$. In scheme 3, we have fixed the orientation of single-ion anisotropy along the laboratory X – Y plane. We have studied the variation in the molecular anisotropies in these schemes for ground and excited eigenstates and presented the

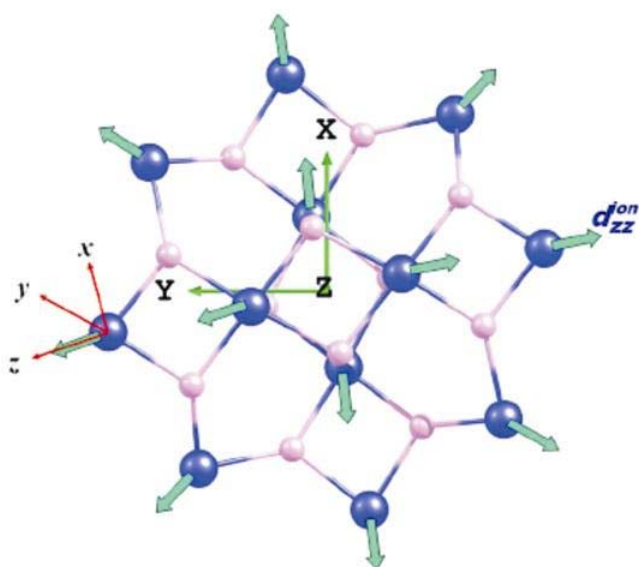


Figure 10. Schematic diagram showing the directions of local anisotropy in Mn_{12}Ac . The z -component of the single-ion anisotropies of all the Mn ions are directed along the plane perpendicular to the laboratory Z axis (scheme 3).

results in table 4. We note that when the local anisotropies are systematically varied, there is a very large variation in the molecular anisotropy as a function of the local orientation (figure 11). The variation of D_M with θ follows the equation $D_M(S) = D_M^0(S)(3\cos^2\theta - 1)$. We find this in all the eigenstates of Mn_{12}Ac that we have studied. The molecular anisotropy values are different in different spin eigenstates. This may be rationalized from the fact that the energy gaps between the ground and the excited states are large as a consequence of which the spin correlations in these states are very different. From the eigenvectors of the $D^{(M)}$ matrix, we find that the choice of our laboratory frame we have chosen is very close to the principal axis of the molecular system in all cases.

We have also studied the role of magnetic orientations of the core Mn(IV) ions ($s = 3/2$) and the crown Mn(III) ions ($s = 2$) in determining the molecular anisotropies by fixing the single ion anisotropy directions of the crown Mn(III) ions fixed at 0° and rotating only the orientation of the anisotropy direc-

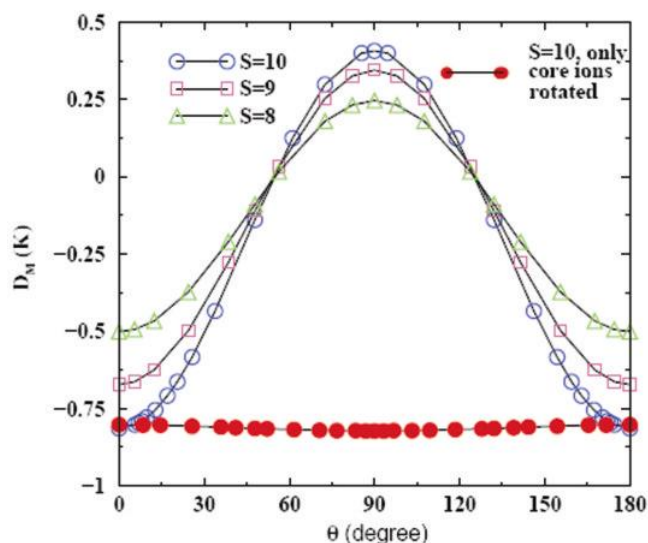


Figure 11. Variation of D_M as a function of θ , the angle the z -component of local anisotropy of Mn(III) ions makes with the laboratory Z -axis in eigenstates with total spin 10, 9 and 8. The orientation of Mn(IV) ions is kept fixed at $\sim 48^\circ$ from the molecular Z -axis. The curve with filled circles correspond to the variation of D_M , when the local anisotropies of the core Mn(IV) ions only are rotated and those of Mn(III) ions are fixed along the Z -axis. The variation of D_M with θ follows the equation $D_M(S) = D_M^0(S)(3\cos^2\theta - 1)$, with all $D_M^0(10) = -0.40$, $D_M^0(9) = -0.34$, $D_M^0(8) = -0.25$. Schemes 1, 2 and 3 correspond to $\theta = 0^\circ$, 17° and 90° . Best fit for the experimental D_M value in the $S_{\text{total}} = 10$ state corresponds to $\theta \sim 17^\circ$.

Table 4. D_M values of ground and excited states of Mn_{12}Ac under various schemes in K. For scheme 2, we have presented the D_M values only for $\theta \sim 17^\circ$ for which the D_M value of the ground state matches with the experimentally observed value.

State	D_M (K)		
	Scheme 1	Scheme 2	Scheme 3
Ground state ($S = 10$)	-0.8138	-0.7083	0.4075
First excited state ($S = 9$) $E_g = 35.1$ K	-0.6722	-0.6105	0.3449
Second excited state ($S = 8$) $E_g = 60.4$ K	-0.5009	-0.4264	0.2464

Table 5. Energy gaps (Δ) and D_0 values for the $S = 10$ ground state corresponding to different sets of parameter values in Mn_{12}Ac .

S. No.	J_1 (K)	J_2 (K)	J_3 (K)	J_4 (K)	Δ (K)	D_0 (K)
1	215	85	85	-64.5	35.1	-0.40
2	215	85	85	-85	67.0	-0.43
3	215	85	64.5	-64.5	72.7	-0.46
4	215	85	45	-45	80.0	-0.49
5	215	85	-85	-45	224	-0.58

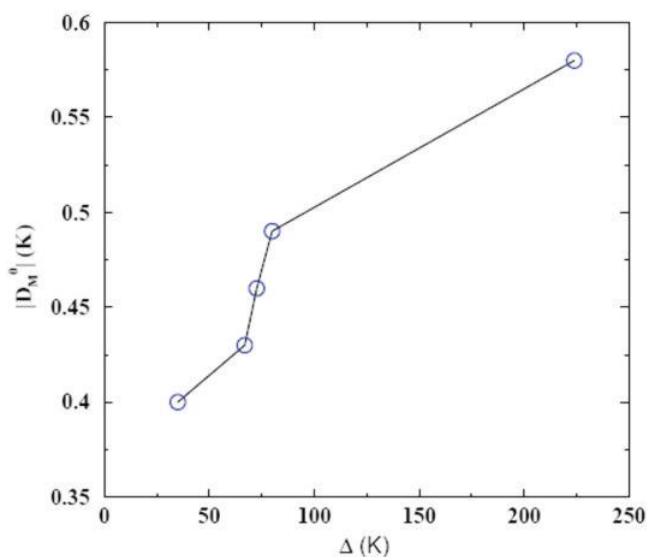


Figure 12. Variation of $|D_M^0|$ as a function of energy gap (Δ in K) for the $S^{\text{total}} = 10$ ground state of Mn_{12}Ac for parameters listed in table 5, $D_M(\theta)$ is given by $-|D_M^0|(3\cos^2\theta - 1)$.

tions of the core Mn(IV) ions systematically. The variation of D_M for the $S = 10$ ground state as a function of rotation of the local anisotropies of the core Mn(IV) ions is shown in figure 11. We observe that the molecular anisotropy is insensitive to the orientations of the core Mn(IV) ions while the orientation of the crown Mn(III) ions control the variation of the molecular magnetic anisotropy in Mn_{12}Ac . In

Mn_{12}Ac , the $S_X^2 - S_Y^2$ term of the anisotropy Hamiltonian does not commute with the D_{2d} molecular point group symmetry and hence E_M is zero. To investigate the variation of D_M^0 with the exchange parameters of the unperturbed Hamiltonian, we have computed the magnetic anisotropy of Mn_{12}Ac in the ground state using five different sets of exchange constants.⁶ In each case, the ground state has spin $S_{\text{total}} = 10$ and the first excited state corresponds to $S = 9$; but the gap to the lowest excited spin state varies (table 5). We see that there is a steady increase in $|D_M^0|$ with increasing gap (see figure 12).

3.2b Magnetic anisotropy in Fe_8 SMM: We have also computed the values of molecular anisotropy for the Fe_8 SMM. First we solve the unperturbed Hamiltonian in (11) by using exchange parameters, $J_1 = 150$ K, $J_2 = 25$ K, $J_3 = 30$ K, $J_4 = 50$ K (figure 13).⁶ The ground state of the system corresponds to total spin $S = 10$ with a $S = 9$ state at 13.56 K, a $S = 9$ state at 27.28 K and a $S = 8$ state at 28.33 K above the ground state. We have computed the magnetic anisotropy of Fe_8 in three different schemes (schemes 4, 5 and 6, figures 14, 15 and 16) similar to Mn_{12}Ac , taking the single ion axial and rhombic anisotropy values for Fe(III) centers to be 1.96 K and 0.008 K respectively. We have studied the variation in the molecular anisotropies as a function of orientation of local anisotropy in these schemes for ground and the excited eigenstates (figure 17).

We have presented the D_M values for the ground and the excited spin states under various schemes in table 6. We note that the molecular anisotropy changes significantly when the local anisotropies are systematically varied (figure 17), in all the eigenstates that we have studied. We also note that given the orientations of local anisotropies, the actual molecular anisotropy values are not very different in different spin eigenstates, since the energy gaps between the ground and the excited states are small which in turn imply that the spin correlations in these states are not significantly different. The ori-

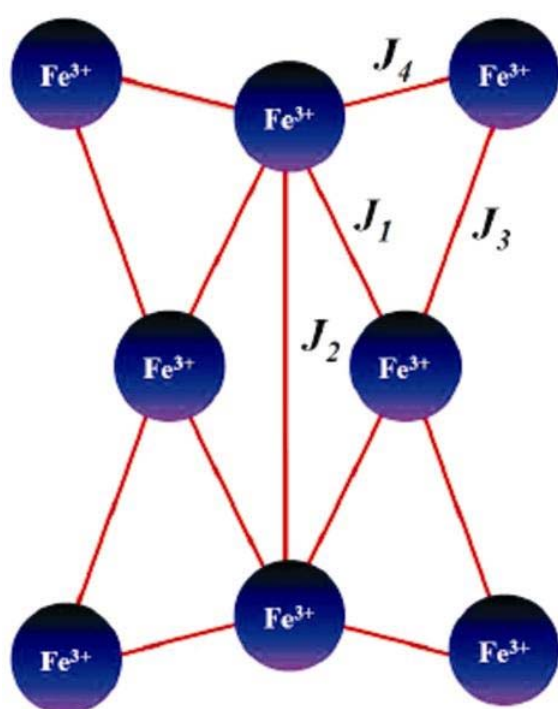


Figure 13. Schematic of exchange interactions in Fe_8 SMM. J_s are the strength of superexchange interaction with $J_1 = 150$ K, $J_2 = 25$ K, $J_3 = 30$ K, $J_4 = 50$ K.⁹

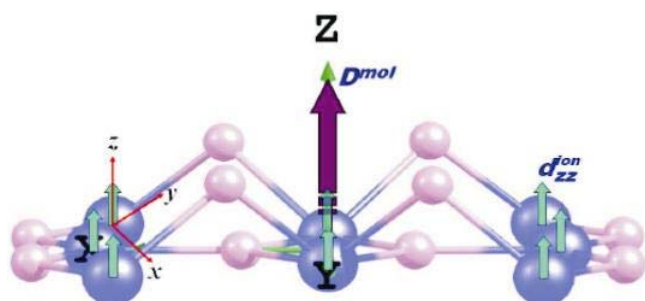


Figure 14. Schematic diagram showing the directions of local anisotropy in Fe_8 . The single-ion anisotropies of all the Fe(III) ions are directed along the laboratory Z -axis (scheme 4).

entation of the local anisotropy centers for which we get the best agreement with experiments ($D_M = -0.28$ K) corresponds to $\theta \sim 82^\circ$.^{35,36} As with Mn_{12}Ac , we find that the laboratory frame we have chosen is very close to molecular axis in all the cases. In case of Fe_8 cluster, the D_2 symmetry commutes with the Hamiltonian in (10) and allows for a non-zero E_M term. The variation of E_M as a function of θ is shown in figure 18, the value of E_M for which D_M has the best fit is 0.017 K compared to the experimental estimate of 0.046 K obtained from High-frequency EPR measurements.³² In this case also, we have explored the variation of D_M^0 with the exchange constants in the unperturbed Hamiltonian (11).⁶ Unlike

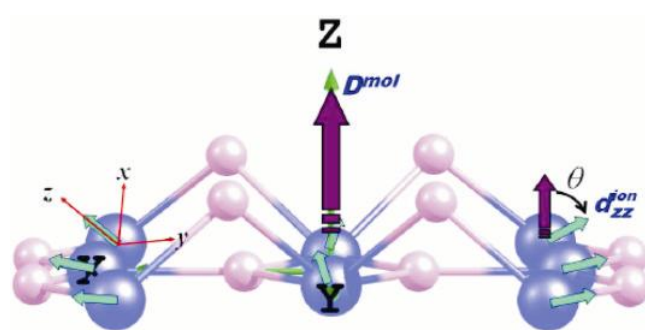


Figure 15. Schematic diagram showing the directions of local anisotropy in Fe_8 . The z -component of the single-ion anisotropies of all the Fe(III) ions are inclined at an angle θ to the laboratory Z -axis (scheme 5).

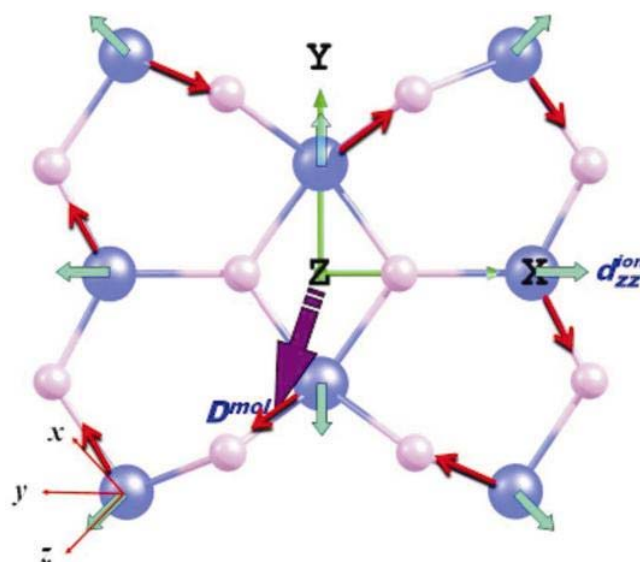


Figure 16. Schematic diagram showing the directions of local anisotropy in Fe_8 . The z -component of the single-ion anisotropies of all the Fe(III) ions are directed along the plane perpendicular to the laboratory Z -axis (scheme 6). The arrows indicate the Fe-O bonds on which the chosen local x -axis has maximum projection.

Table 6. D_M values of ground and excited states of Fe_8 under schemes 4, 5 and 6 in K. For scheme 5, we have presented the D_M values only for $\theta = 82.2^\circ$ for which the D_M value of the ground state matches with the experimentally observed value. Experimental D_M values are given in parenthesis and the corresponding references in square brackets.

State	D_M (K)		
	Scheme 4	Scheme 5	Scheme 6
Ground state ($S = 10$)	0.6030	-0.2867 (0.28) ³²	-0.3033
First excited state ($S = 9$) $E_g = 13.56$ K	0.5821	-0.2763 (-0.27) ³⁷	-0.2923
Second excited state ($S = 9$) $E_g = 27.28$ K	0.5877	-0.2790 (-0.27) ³⁷	-0.2952
Third excited state ($S = 8$) $E_g = 28.33$ K	0.5503	-0.2607	-0.2758

Table 7. Energy gaps (Δ) and D_0 values for the $S = 10$ ground state corresponding to different sets of parameter values in Fe_8 .

S. No.	J_1 (K)	J_2 (K)	J_3 (K)	J_4 (K)	Δ (K)	D_0 (K)
1	180	153	22.5	52.5	5.87	0.30
2	150	25	30	50	13.56	0.30
3	195	30	52.5	22.5	41.40	0.30
4	201	36.2	58.3	26.1	42.5	0.30

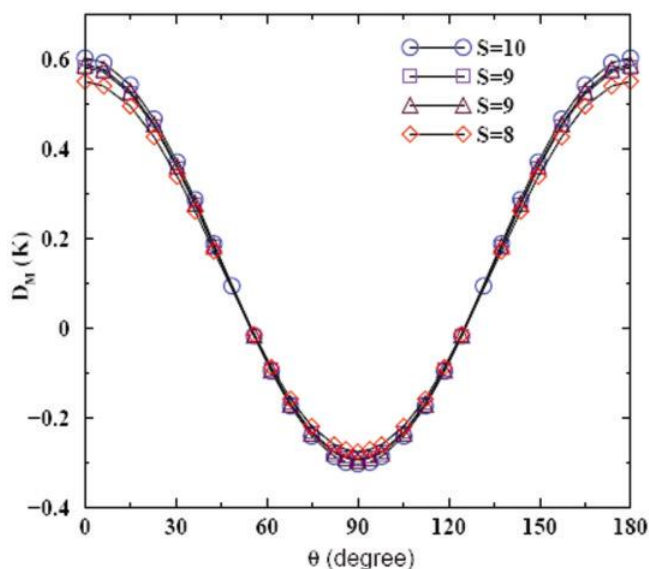


Figure 17. Variation of D_M in Fe_8 cluster as a function of θ , the angle the z -component of local anisotropy of Fe(III) ions makes with the laboratory Z -axis. All the plots can be fitted to $D_M^0(S)(3\cos^2\theta - 1)$, with $D_M^0(10) = 0.3$, $D_M^0(9) = 0.29$, $D_M^0(8) = 0.275$. $D_M^0(S)$ is almost independent of S . Best fit for the experimental D_M value in the $S_{\text{total}} = 10$ state corresponds to $\theta \sim 82^\circ$.

with Mn_{12}Ac , we find that D_M^0 is almost independent of the excitation gap of the exchange Hamiltonian (table 7).

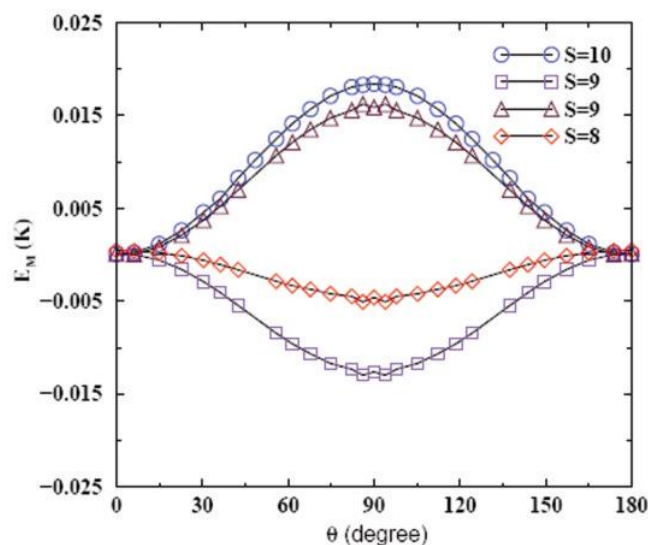


Figure 18. Variation of E_M in Fe_8 cluster as a function of θ , the angle the z -component of local anisotropy of Fe(III) ions makes with the laboratory Z -axis for scheme 5.

4. Conclusions

In this paper we presented a hybrid technique based on constant M_S basis and VB basis which adapts both spin and spatial symmetry of a general point group. This technique can be used to obtain the eigenstates of spin and electronic model Hamiltonians with any molecular point group symmetry. We

also presented general method to calculate the molecular magnetic anisotropy parameters, D_M and E_M for single molecule magnets in a chosen eigenstate of the exchange Hamiltonian. The molecular anisotropies are computed from the single-ion anisotropies, using first order perturbation theory for different spin states of the SMMs. We have computed the molecular magnetic anisotropy parameters of $Mn_{12}Ac$ and Fe_8 SMMs in various eigenstates of different total spin. We have also studied the variation of molecular anisotropy with the orientation of the local anisotropy of the metal ions. In $Mn_{12}Ac$ and Fe_8 clusters, we find that the molecular anisotropy changes drastically with the local anisotropy direction. In $Mn_{12}Ac$, the D_M value is different in ground and excited states we have computed, owing to large difference in spin–spin correlation values. The molecular anisotropy of $Mn_{12}Ac$ does not change significantly with the orientation of the local anisotropy of the core Mn(IV). D_M value in Fe_8 is not very different in ground and excited states probably due to small energy gaps which implies similar spin–spin correlations which is in consistent with the magnetic anisotropies computed for different sets of exchange constants. We find that in $Mn_{12}Ac$, the anisotropy constants increase significantly with the gap, while in Fe_8 they are almost independent of the gap. In $Mn_{12}Ac$, the first order rhombic anisotropy term is zero due to the D_{2d} symmetry of the molecule while it is non-zero in Fe_8 .

References

1. Thomas L, Lioni F, Ballou R, Gatteschi D, Sessoli R and Barbara B 1996 *Nature* **383** 145
2. Linert W and Verdager M 2003 *Molecular magnets: Recent highlights* (New York: Springer-Verlag)
3. Miller J S and Drillon M 2003 *Magnetism: Molecules to materials IV* (Wiley-VCH Verlag GMBH)
4. Shoji M, Koizumi K, Hamamoto T, Kitagawa Y, Yamanaka S, Okumura M and Ya-Maguchi K 2006 *Chem. Phys. Lett.* **421** 483
5. Sessoli R, Gatteschi D, Caneschi A and Novak M A 1993 *Nature* **365** 141
6. Raghun C, Rudra I, Sen D and Ramasesha S 2001 *Phys. Rev.* **B64** 064419
7. Rudra I, Ramasesha S and Sen D 2002 *Phys. Rev.* **B66** 014441
8. Pati S, Ramasesha S and Sen D 2002 *Magnetism: Molecules to materials IV* (eds) J S Miller and M Drillon (Wiley-VCH)
9. Sahoo S, Rajamani R, Ramasesha S and Sen D 2008 *Phys. Rev.* **B78** 054408
10. Pauncz R 1979 *Spin eigenfunctions: Construction and use* (New York: Plenum Press)
11. Ramasesha S and Soos Z G 1993 *J. Chem. Phys.* **98** 4015
12. Pauling L 1933 *J. Chem. Phys.* **1** 280
13. Pauling L and Wheland G W 1933 *J. Chem. Phys.* **1** 362
14. Soos Z and Ramasesha S 1990 *Valence bond theory and chemical structure* (eds) D J Klein and N Trinajstić (New York: Elsevier)
15. Ramasesha S and Soos Z 2002 *Valence bond theory* (ed.) D L Cooper (New York: Elsevier)
16. Arovas D, Auerbach A and Haldane F 1988 *Phys. Rev. Lett.* **60** 531
17. Bishop D 1973 *Group theory and chemistry* (Oxford: Clarendon Press)
18. Wang S, Zuo J-L, Zhou H-C, Choi H, Ke Y, Long J R and You X-Z 2004 *Angew. Chem. Int. Ed.* **43** 5940
19. Kahn O 1993 *Molecular magnetism* (New York: VCH Publishers Inc.)
20. Oudar J L and Zyss J 1982 *Phys. Rev.* **A26** 2016
21. Bencini A, Benelli C and Gatteschi D 1984 *Coord. Chem. Rev.* **60** 131
22. Bencini A and Gatteschi D 1990 *EPR of exchange coupled systems* (Berlin: Springer)
23. Pederson M and Khanna S 1999 *Phys. Rev.* **B60** 9566
24. Pederson M, Kortus J and Khanna S 2002 *J. Appl. Phys.* **91** 7149
25. Kortus J, Baruah T, Bernstein N and Pederson M 2002 *Phys. Rev.* **B66** 092403
26. Takeda R, Mitsuo S, Yamanaka S and Yamaguchi K 2005 *Polyhedron* **24** 2238
27. Takeda R, Koizumi K, Shoji M, Nitta H, Yamanaka S, Okumura M and Yamaguchi K 2007 *Polyhedron* **26** 2309
28. Neese F and Solomon E 1998 *Inorg. Chem.* **37** 6568
29. Carrington A and McLachlan A 1967 *Introduction to magnetic resonance: With applications to chemistry and chemical physics* (New York: Harrer and Row Publishers)
30. Ramasesha S and Soos Z G 1984 *Chem. Phys.* **91** 35
31. Barra A L, Gatteschi D and Sessoli R 2000 *Chem. Eur. J.* **6** 1608
32. Barra A-L, Debrunner P, Gatteschi D, Schulz C E and Sessoli R 1996 *Europhys. Lett.* **35** 133
33. Cornia A, Sessoli R, Sorace L, Gatteschi D, Barra A L and Daiguebonne C 2002 *Phys. Rev. Lett.* **89** 257201
34. Barra A L, Gatteschi D, Sessoli R, Abbati G L, Cornia A, Fabretti A C and Uytterhoeven M G 1997 *Angew. Chem. Int. Ed. Engl.* **36** 2329
35. Accorsi S, Barra A, Caneschi A, Chastanet G, Cornia A, Fabretti A C, Gatteschi D, Mortalo G, Olivieri E, Parenti F, Rosa P, Sessoli R, Sorace L, Wernsdorfer W and Zobbi L 2006 *J. Am. Chem. Soc.* **128** 4742
36. Heerd T P, Stefan M, Goovaerts E, Caneschi A and Cornia A 2006 *J. Mag. Res.* **179** 29
37. Zipse D, North J, Dalal N, Hill S and Edwards R 2003 *Phys. Rev.* **B68** 184408